PERGAMON

International Journal of Heat and Mass Transfer 45 (2002) 57–65

International Journal of HEAT and MASS TRANSFER

www.elsevier.com/locate/ijhmt

Heat transfer in condensing, pulsating flows

Scott E. Hommema [a,*], Keith A. Temple [b], James D. Jones [a], Victor W. Goldschmidt [a]

[a] *Ray W. Herrick Laboratories, Purdue University, West Lafayette, IN 47907, USA*
[b] *Lennox Industries Inc., Carrollton, TX 75011, USA*

Received 19 September 2000; received in revised form 2 April 2001

Abstract

The internal heat transfer coefficient in a pulsating circular pipe flow was determined for both dry and condensing surfaces. The fully-reversing flow was driven by a pulse combustion process at a frequency of 34 Hz. The mean Reynolds numbers ranged from approximately 2600 to 4300, while the instantaneous Reynolds number had a maximum of 18,000. The internal heat transfer is noted to increase by up to a factor of 1.8 due to the pulsating flow prior to the onset of condensation, and by up to 12 times after the onset of condensation. At all Reynolds numbers and flow regimes tested, the flow pulsations were observed to enhance heat transfer when compared to steady flow results.

1. Introduction

The main motivation for the study now reported was the need for determining the heat transfer for circular tubes in the heat exchanger of a pulse combustion heating system. It has been theoretically suggested, and experimentally shown, that under certain conditions, heat transfer may be enhanced by flow pulsations [1]. Under other conditions, however, some researchers have observed that flow pulsations have either no effect or a detrimental effect, on heat transfer. Dec et al. [2] provides a review of studies dealing with heat transfer in pulsating flow. An additional review of pertinent literature follows.

Barnett and Vachon [3], in their experiments with pulsating turbulent pipe flow, found that high frequency pulsations degraded heat transfer, and low frequency pulsations enhanced heat transfer. They reasoned that the observed enhancement was due primarily to the promotion of turbulence. Celik and Wang [4] came to a similar conclusion: low frequency flow pulsations promote the formation of local turbulence which breaks up the boundary layers, thereby enhancing heat transfer. Al-Haddad and Al-Binally [5], while correlating their data from experiments with pulsating flow of air in a pipe, defined a dimensionless number as the product of the Reynolds number and a dimensionless frequency. A critical value for this parameter was experimentally determined, and it was observed that operating the apparatus above this critical value resulted in heat transfer enhancement, while operating below this value showed no change from their steady-flow predictions of heat transfer.

Hargrave et al. [6] performed experiments on a pulse combustion water heater with pulsation frequencies in the range of 30–40 Hz. Their results indicate a factor of two improvement in heat transfer for velocity amplitudes of four times the mean value. A similar apparatus was used by Al-Haddad and Coulman [7] at a frequency range of 45–60 Hz to investigate the effect of mass flow on heat transfer enhancement. Their results indicated a degradation in heat transfer for all flow rates and frequencies. They concluded, however, that "no statement could be generalized and more study is required".

Additional researchers who observed enhanced heat transfer in pulsating systems include Hanby [8],

* Corresponding author. Present address: Laboratory for Turbulence and Complex Flow, University of Illinois, 216 Talbot Laboratory, 104 S. Wright St., Urbana, IL 61801, USA. Tel.: +1-217-333-4264; fax: +1-217-244-5707.

E-mail address: shommema@uiuc.edu (S.E. Hommema).

0017-9310/02/$ - see front matter
PII: S0017-9310(01)00132-6

Nomenclature

b_{1n}, b_{2n}, b_{3n}	Gray gas model coefficients
C_1, C_2	Zhukauskas coefficients
c_p	specific heat at constant pressure
D	pipe diameter
g	acceleration of gravity
h	heat transfer coefficient
j_{fg}	specific latent heat of vaporization
j'_{fg}	effective specific latent heat of vaporization
k	thermal conductivity
L	pipe length
Nu	Nusselt number
Pr	Prandtl number $(= c_p\mu/k)$
p	partial pressure
q''	heat flux
r	pipe radius
Re_D	mean Reynolds number based on pipe diameter
T	temperature
U	axial velocity
z	axial coordinate

Greek symbols

α	absorptivity
ε	emissivity
ρ	density
γ	dimensionless length $(= z/L)$
μ	dynamic viscosity
ν	kinematic viscosity $(= \mu/\rho)$
σ	Stefan–Boltzmann constant
τ	pulsation period
ω	pulsation frequency

Subscripts

a	amplitude
CO_2	carbon dioxide
D	diameter
e	external
f	film
g	gaseous phase
H_2O	water vapor
i	internal
l	liquid
m	mean
rad	radiative
s	surface
sat	saturation
v	vapor phase
∞	ambient/reference

Gemmen et al. [9,10], and Dec and Keller [11]. Arpaci et al. [12] correlated the experimental data of Dec and Keller [11] to develop an expression for the Nusselt number in pulsating, reversing flow. This correlation incorporates the effect of pulsation amplitude, pulsation frequency, and Reynolds number based on mean velocity. Their correlation gives remarkable agreement with the data of Dec and Keller [11] at all frequencies and mass flow rates considered. Included in the development is discussion of a quasi-steady frequency limit. The authors suggest that at frequencies below this value (46 Hz), a quasi-steady theory could be used to adequately predict heat transfer. Beyond this limit, quasi-steady predictions of heat transfer were shown to underestimate the data of Dec and Keller [11].

The correlation of Arpaci et al. [12] was applied by Temple [13] to the modeling of heat transfer from a quarter-wave pipe subject to internal pulsating flow. Included in this work is a semi-empirical treatment of the effects of bends on internal heat transfer. Model predictions were compared with experimental data taken above and below the quasi-steady limit showing excellent agreement in overall heat transfer. Predicted internal and surface temperatures showed good agreement with experimental data as well. The comprehensive pulse combustion model of Temple [13] also used the correlation of Arpaci et al. [12] to determine heat transfer coefficients for flow within the tailpipe and combustion chamber of a pulse combustion furnace.

Although some experimental evidence suggests otherwise, it appears that heat and mass transfer is enhanced by flow reversals [2]. Pulsating flow with flow reversals of sufficient magnitude will result in heat transfer greater than that for steady flow. The parameters governing this enhancement and the mechanisms by which it occurs are still unresolved.

The literature is rich with studies of heat transfer in steady (non-pulsating), two-phase flows. [1] Amongst them are the heat transfer correlations of Akers and Rosson [15], Chato [16], Bae et al. [17], Traviss et al. [18], and Jaster and Kosky [19]. Although a wide body of literature exists in the area of condensation inside tubes, studies related to condensing pulsating flows were not found. It is the aim of the present work to begin to fill that gap.

2. Experimental apparatus

The experimental apparatus is sketched in Fig. 1. A pulse combustion furnace, based on a Helmholtz res-

[1] A more complete literature review is available in [14].

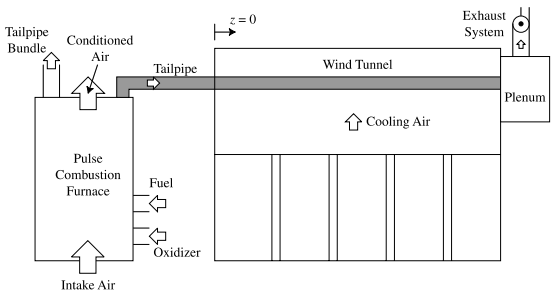

Fig. 1. Condensation heat transfer experimental apparatus. A natural gas fired pulse combustion furnace drives the fully reversing flow in the tailpipe. The mean flow of combustion products in the tailpipe is from left-to-right. The wind tunnel provides a uniform cooling stream over the tailpipe.

onator, and designed for residential forced-air heating, was used to establish a pulsating, fully reversing velocity field within a parallel network of serpentine tailpipes fed from a common manifold. As shown in Fig. 2, one such tailpipe was replaced with a straight tailpipe of equal length. Each tailpipe of the furnace expels an equal fraction of the combustion products which consist mostly of nitrogen, carbon dioxide, and water vapor. If the gas in the pipes is sufficiently cooled, the water vapor will condense.

The single, straight tailpipe was constructed from stainless steel tubing of 19.05 mm outside diameter and 0.89 mm wall thickness. Section 1 of the tube was outfitted with external annular fins while Sections 2 and 3 had no external heat transfer enhancements. This unfinned tubing (Sections 2 and 3) became the test section and was placed in cross-flow in the open-air wind tunnel shown in Fig. 3. The five blowers were set to deliver 6.6 ± 0.3 m s^{-1} flow across the centerline of the test section. We will adopt a coordinate system with the left edge of the wind tunnel as the $z = 0$ datum. An exhaust system was required to prevent build-up of gaseous combustion products in the laboratory. The open end of the test section was fed into a large plenum. An exhaust fan removed the gases from the plenum and expeled them through a duct to the outside. Further information regarding the experimental apparatus is available from [14].

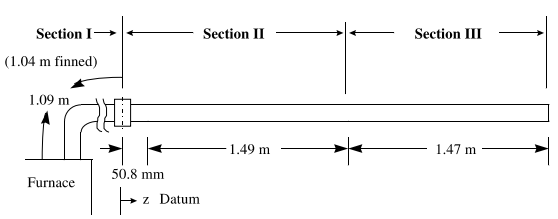

Fig. 2. Horizontal tailpipe (test section).

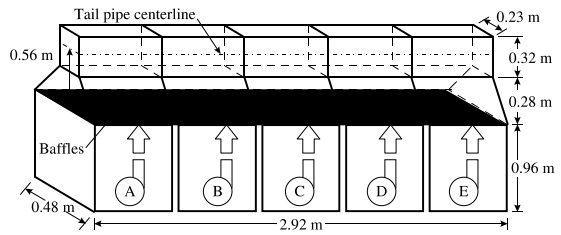

Fig. 3. Schematic of vertical wind tunnel. Five independent blowers are used to generate the external flow field. A series of baffles and screens conditions the stream before it is passed over the heated horizontal pipe.

The mass flow rate of the natural gas (fuel) was determined from volumetric flow rate measurements, using a positive displacement gas meter. The mass flow rate of combustion air (oxidizer) was computed based upon the measured flow rate of fuel and an air-to-fuel ratio determined through oxygen concentration measurements in the exhaust. Condensate flow rates were determined by collecting the condensate at the end of the tube over a sufficiently long time interval and measuring the total mass collected.

All temperature measurements were made using K-type (chromel–alumel) thermocouples. The horizontal tailpipe was outfitted with a surface welded thermocouple and a probe-type thermocouple as shown in Fig. 4 at each of 15 axial locations along the pipe. Internal gas temperatures were measured using specially constructed probes. These probes used 0.3 mm diameter thermocouple junctions composed of 0.076 mm diameter chromel–alumel wire. The thermocouple leads were housed in a ceramic sheath and mounted at each measurement location as shown in Fig. 4. These probe thermocouples were designed to present minimal blockage to the internal flow and were mounted such that their ceramic sheath was flush with the inner wall of the pipe. The thermocouple bead was located 5 ± 1 mm from the inner surface of the pipe leaving only the thermocouple junction and the thin lead wires exposed to the flow. Additional shielded thermocouple probes for which the ceramic shield extended past the sensor head, were constructed for use within regions of the test section where condensate was present to prevent

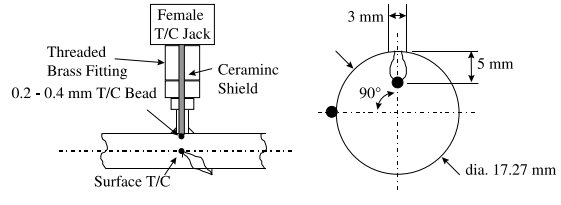

Fig. 4. Schematic of sensors used to measure surface and internal gas temperatures.

moisture from impacting the sensors and generating erroneous readings.

Specialized sensors were developed to detect liquid condensate film within the two-phase regions of the horizontal tailpipe. These sensors were based on the work of Lyu and Mudawar [20], and are similar in principle to a hot-wire anemometer operating in a constant current configuration (see Fig. 5). Its operation can be understood by considering a situation where a portion of the wire (Pt–10% Rh) is covered with a condensate film and the remainder is exposed to a gas flow. Assuming the gas and liquid are at the same temperature, the portion of the wire exposed to the liquid film will experience a larger convective heat flux due to the increased thermal conductivity of water. The change in heat transfer, and resultant change in wire temperature will alter the resistance of the sensor. This resistance change was monitored by measuring the voltage across the sensing element. Measurements in this study were obtained with a mean value of 200 mA of current through the sensor wire, supplied by a constant current DC power supply.

Experimental uncertainties for each measured physical parameter are summarized in Table 1. Also included are the uncertainties in computed quantities such as total mass flow rate, composite heat transfer coefficient, Nusselt number, and Reynolds number. These uncertainties account for the accuracy of the measuring instruments, errors associated with the data acquisition, uncertainties in sensor location, and measurement repeatability and represent the maximum anticipated uncertainty.

Transient pressures were measured using quartz charge-coupled dynamic pressure transducers mounted in water-cooled housings. Pressure measurements obtained in the combustion chamber were used to determine the fundamental pulsation frequency of the pulse combustion unit and provided a convenient time reference.

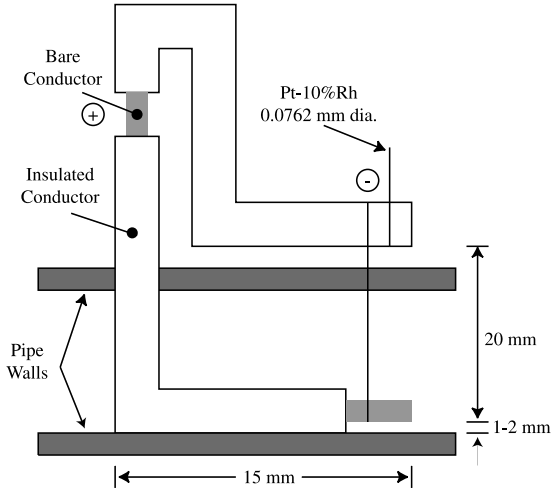

Fig. 5. Condensate film sensor.

Table 1
Experimental uncertainties

Parameter	Uncertainty
Measured quantities	
Exhaust oxygen concentration	5% of reading
Gas mass flow rate	±1%
External air velocity	±0.2 m s^{-1}
Temperature	Greater of 0.75% or ±2.2°C
Condensate mass flow rate	±3%
Dynamic pressure	Greater of 2.0% or 0.03 kPa
Computed quantities	
Total mass flow rate	±4%
Dew point	±2°C
Composite heat transfer coefficient	±12%
Nusselt number	±12%
Reynolds number	±4%

3. Experimental results

Measurements were taken at eight different input rates as summarized in Table 2. The data which follows are presented in terms of a dimensionless axial (streamwise) coordinate, ($\gamma = z/L$).

Mean gas temperatures at 15 locations along the test section are shown in Fig. 6 at each of the eight input (mass flow) rates. Radial traverses at a number of axial locations revealed relatively flat mean temperature profiles so a single internal gas temperature was used to characterize the cross-section at each axial location of interest. Mean surface temperatures for the same experimental runs are shown in Fig. 7. Circumferential temperature measurements taken at a number of axial locations indicated a flat profile and justified the use of a single surface temperature measurement to characterize the cross-section.

Referring to Fig. 7, we may identify three different heat transfer regimes in the test section. The first, $0 < \gamma < 0.5$, shows an exponential decrease in surface temperature characteristic of single-phase, forced convection heat transfer. The second region, $0.5 < \gamma < 0.8$, is characterized by constant surface temperature signifying a phase change process – in this case, condensation heat transfer. The third region, $\gamma > 0.8$, is characterized by a decreasing surface temperature. The authors theorize that this decrease is due to the transition to a different two-phase flow regime where the breakup and entrainment of the liquid condensate film results in en-

Table 2
Operating characteristics of pulse combustion furnace for various input rates

Parameter	Operating characteristics							
Input rate (kW)	24.4	23.5	22.7	21.5	20.7	20.0	18.9	16.9
Gas orifice diameter (mm)	3.99	3.91	3.86	3.73	3.66	3.57	3.45	3.26
Gas flow rate (g s^{-1})	0.410	0.395	0.383	0.361	0.349	0.336	0.319	0.284
Air flow rate (g s^{-1})	8.49	8.22	8.14	8.10	7.95	7.70	7.53	7.49
Air-to-fuel ratio (dimensionless)	20.7	20.8	21.1	22.0	22.8	22.9	23.6	26.4
Condensate flow rate[a] (g s^{-1})	0.041	0.034	0.029	0.033	0.033	0.027	0.031	0.022
Total condensate flow rate[b] (g s^{-1})	0.51	0.44	0.47	0.41	0.41	0.40	0.38	0.32
Exhaust CO_2 (%)	9.64	9.58	9.41	9.03	8.68	8.63	8.35	7.42
Pulse frequency (Hz)		34.1						

[a] Condensate mass flow in single horizontal tailpipe under consideration.
[b] Combined condensate mass flow from furnace and tailpipe.

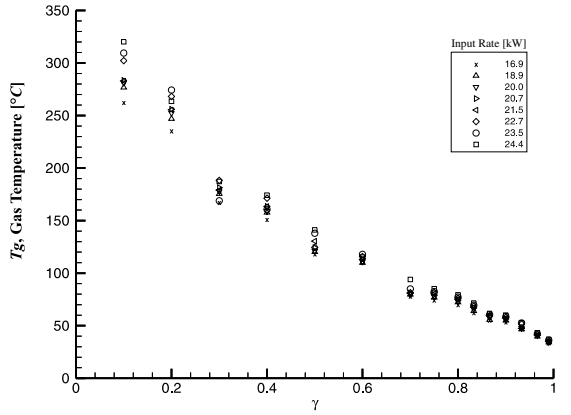

Fig. 6. Mean gas temperature as a function of dimensionless axial coordinate at eight different mass flow rates.

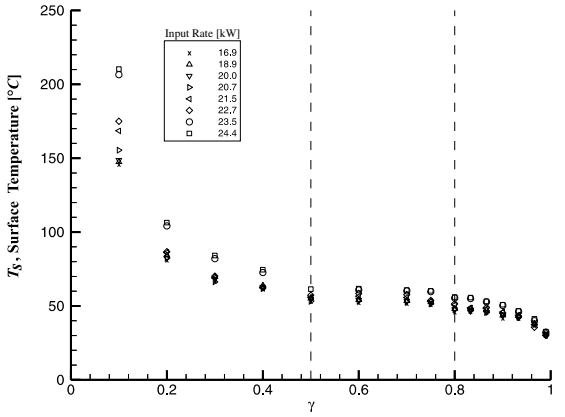

Fig. 7. Mean surface temperature as a function of dimensionless axial coordinate at eight different mass flow rates.

hanced heat transfer (further discussed in the sections which follow).

Fig. 8 shows three sample traces from the liquid film sensor. A 34 Hz periodicity is difficult to discern due to the noise level. Fourier decompositions (ffts) of the voltage traces did, however, reveal a clear 34 Hz component. The trace taken at $\gamma = 0.99$, where the flow was undoubtedly two-phase, indicates an additional feature. The increased levels of high frequency "noise" suggest the influence of condensate film and droplets as they impact the sensor wire. The time base for the sensor traces is determined from a simultaneous record of the combustion chamber pressure, and $\tau = 0$ corresponds to a pressure maximum.

Two-phase flow regime maps [2] based on steady flow would predict an annular flow regime for the conditions of this study. A separate visualization experiment (not reported here) for which Section 3 of the straight pipe

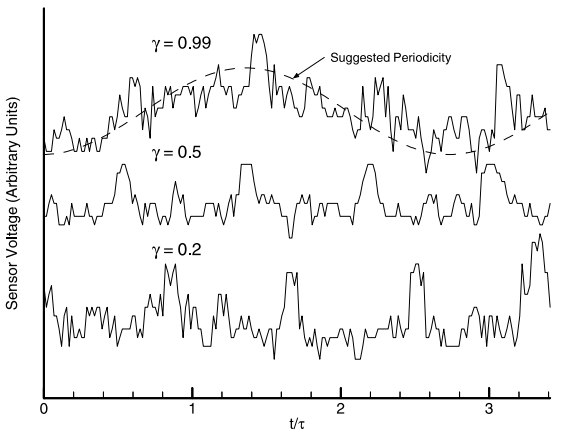

Fig. 8. Traces from the condensate film sensor at three locations for an input rate of 23.5 kW.

[2] cf. [21] for a map based on steady flow suitable for horizontal ducts at atmospheric pressure. No flow map based on pulsating flow exists to the author's knowledge.

was replaced with a clear section, did not indicate a liquid annulus on the interior perimeter of the pipe. Rather, the moisture was present in the form of large

drops on the surface of the pipe which would grow, separate from the wall, and become entrained in the interior bulk flow. A cloud or mist of small suspended droplets was observed in the centre of the pipe.

The mean value of the voltage signal is observed to vary from a local minimum near the start of the trace to a local maximum near 1.36 pulsation periods and returns to a minimum near 2.73 pulsation periods. Such large scale periodicity may be indicative of the buildup and subsequent breakdown of condensate droplets (or films) near the sensor. Further study, including improved visualization, is required for confirmation.

4. Heat transfer characterization

The heat transfer per unit surface area can be determined along the pipe at any axial location by focusing on the interior of the pipe

$$q''_{\mathrm{i}} = h_{\mathrm{i}}(T_{\mathrm{g}}(z) - T_{\mathrm{s}}(z)) + h_{\mathrm{rad,i}}(T_{\mathrm{g}}(z) - T_{\mathrm{s}}(z)), \tag{1}$$

where the composite heat transfer coefficient h_{i} combines both convective and latent terms, or alternatively, by focusing on the exterior of the pipe

$$q''_{\mathrm{e}} = h_{\mathrm{e}}(T_{\mathrm{s}}(z) - T_{\infty}) + h_{\mathrm{rad,e}}(T_{\mathrm{s}}(z) - T_{\infty}). \tag{2}$$

Assuming axial conduction in the thin pipe walls is negligible, we may equate (1) and (2), giving $q''_{\mathrm{i}} = q''_{\mathrm{e}} \equiv q''$.

For the external flow, we compute the heat transfer coefficient using the correlation from Zhukauskas [22], with $C_1 = 0.26$ and $C_2 = 0.6$ for $10^3 < Re_{\mathrm{D}} < 2 \times 10^5$:

$$h_{\mathrm{e}} = \frac{k_{\mathrm{f}}}{D}\left[C_1 Re_{\mathrm{D}}^{C_2} Pr^{0.37}\left(\frac{Pr}{Pr_{\mathrm{s}}}\right)^{0.25}\right]. \tag{3}$$

The velocity of the external cooling air (which appears in Re_{D}), was determined by a series of pitot probe traverses. The operating speed of the four blowers in the wind tunnel were adjusted until a nominally uniform velocity of 6.6 m s^{-1} at the centerline of the tailpipe was attained. Axial and traverse nonuniformities in the external air velocity were less than ± 0.3 m s^{-1}.

The heat transfer coefficient due to external radiation is given by

$$h_{\mathrm{rad,e}} = \sigma\varepsilon_{\mathrm{s}}(T_{\mathrm{s}}^2 + T_{\infty}^2)(T_{\mathrm{s}} - T_{\infty}). \tag{4}$$

The heat transfer coefficient due to internal radiation is evaluated as

$$h_{\mathrm{rad,i}} = \frac{\sigma(\varepsilon_{\mathrm{g}} T_{\mathrm{g}}^4 - \alpha_{\mathrm{g}} T_{\mathrm{s}}^4)}{T_{\mathrm{g}} - T_{\mathrm{s}}}. \tag{5}$$

The emissivity and absorptivity of the gas are determined using the four-term mixed gray gas model developed by Truelove [23] and utilized by Temple [13]. In this model, the emissivity is determined from the partial pressures of water vapor and carbon dioxide using

$$\varepsilon_{\mathrm{g}} = \sum_{n=1}^{4}(b_{1n} + b_{2n}T_{\mathrm{g}})[1 - \exp(-0.0164 b_{3n}(p_{\mathrm{H_2O}} + p_{\mathrm{CO_2}}))]. \tag{6}$$

Similarly, the absorptivity is determined from

$$\alpha_{\mathrm{g}} = \sum_{n=1}^{4}(b_{1n} + b_{2n}T_{\mathrm{s}})[1 - \exp(-0.0164 b_{3n}(p_{\mathrm{H_2O}} + p_{\mathrm{CO_2}}))], \tag{7}$$

with the 12 coefficients as given in the referenced literature [23].

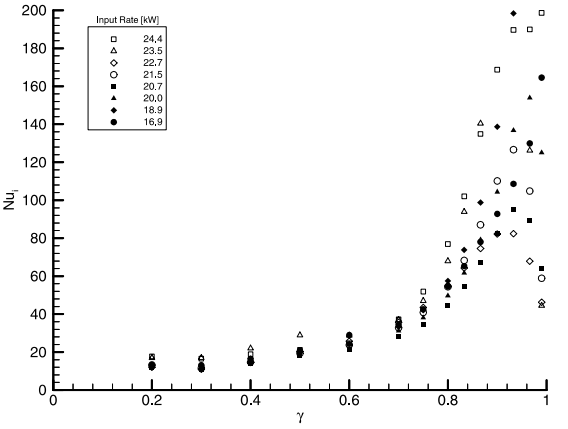

Fig. 9. Variation of measured Nusselt with streamwise coordinate.

Coupled with Eqs. (1)–(7), the measured internal gas and surface temperatures (actually using smooth polynomial fits to mask out experimental uncertainty and noise) are sufficient to compute the unknown composite heat transfer coefficient h_{i}, and in turn Nu_{i}. The results for such a computation are plotted in Fig. 9 as functions of γ. The same data is plotted against mean Reynolds number [3] in Fig. 10 and overlaid with the correlations of Dittus–Boelter for steady single-phase flow,

$$Nu_{\mathrm{D}} = 0.023 Re_{\mathrm{D}}^{0.8} Pr^{0.3}; \tag{8}$$

Arpaci [12] for the case of single-phase, pulsating flow, which when applied to the conditions of the current tests yield

$$Nu_{\mathrm{D}} = \frac{h_{\mathrm{i}} D}{k_{\mathrm{f}}} = 0.028 Re_{\mathrm{D}}^{0.75}\left(1 + 0.21\frac{U_{\mathrm{a}}}{U_{\mathrm{m}}}\right)^{0.75}, \tag{9}$$

[3] One could define a mean and fluctuating (instantaneous) Reynolds number based on the mean and instantaneous bulk velocity, respectively. The Reynolds number used subsequently is based upon pipe diameter and a mean bulk velocity.

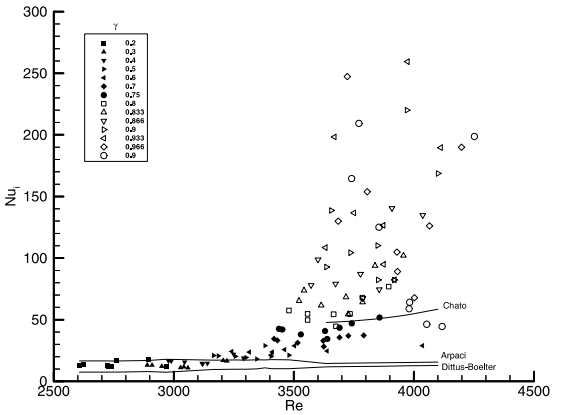

Fig. 10. Comparison of measured Nusselt number with published correlations of Dittus–Boelter [24], Arpaci [12], and Chato [16]. Results are shown as a function of mean Reynolds number.

and the correlation by Chato [16] for filmwise condensation

$$h = 0.555\left[\frac{g\rho_l(\rho_l-\rho_v)k_l^3 j'_{\mathrm{fg}}}{\mu_l(T_{\mathrm{sat,g}}-T_{\mathrm{s}})D}\right]^{1/4}, \tag{10}$$

where the effective latent heat takes the form

$$j'_{\mathrm{fg}} = j_{\mathrm{fg}} + \frac{3}{8}c_{\mathrm{p,l}}(T_{\mathrm{sat,g}}-T_{\mathrm{s}}). \tag{11}$$

Use of the mean Reynolds number allows the four heat transfer regimes (steady/one-phase, steady/two-phase, pulsating/single-phase, and pulsating/two-phase) to be compared for an equal mass flow rate. An extensive set of correlations for steady two-phase flow is available including those from Bae et al. [17], Traviss et al. [18], and Jaster and Kosky [19]. However, they were not used here as they require data such as local quality, pressure gradients, etc. which were not directly measured in the current study.

One notes from Eq. (9) that the velocity amplitude, U_{a}, and mean velocity, U_{m}, are required to predict Nu_{D} for single-phase, pulsating flow using the Arpaci correlation. Although neither parameter was known independently in this study, they appear only as the ratio $U_{\mathrm{a}}/U_{\mathrm{m}}$. This ratio was determined from the pulse combustor model of Temple [13] for the current operating conditions. This ratio was approximately four and varied only 10% over the entire range of input rates.

Averaged heat transfer enhancement results are summarized in Tables 3 and 4 and Fig. 11 which compare the ratios of the experimentally determined composite internal Nusselt number, Nu_{i}, with the aforementioned correlations for steady, single-phase; pulsating, single-phase; and steady two-phase flows, respectively. The temperatures measured at each axial location have been averaged over at least 1000 pulsation periods, over 10 or more ensembles, and over all eight input rates to generate the numbers in Table 4, and subsequently represent mean, rather than instantaneous results. The erroneously high ratio at $\gamma = 0.1$ is most likely due to flow non-uniformities in the external velocity at the edge of the wind tunnel. Therefore, the results for $\gamma = 0.1$ have not been included in the subsequent analyses and discussion. Qualitatively and quantitatively similar results were obtained at all input rates.

Table 3
Experimentally determined Nusselt number along the pipe averaged over all eight input rates

$\gamma = z/L$	Nu_{i}
0.1	34.79[a]
0.2	13.79
0.3	13.20
0.4	16.58
0.5	21.20
0.6	21.52
0.7	33.74
0.75	42.55
0.8	57.55
0.833	72.96
0.866	95.03
0.9	124.91
0.933	149.55
0.966	138.62
0.99	113.91

[a] Value is suspect due to nonuniformity of external flow at measurement location.

An additional correlation for single-phase pulsating flow is available from Al-Haddad and Al-Binally [5]. This correlation is based on the parameter $Re\,\omega'$, where ω' is a dimensionless frequency given by $\omega r^2/v$. Their results indicated that heat transfer was significantly enhanced when $Re\,\omega' > 2.1\times10^5$, and for the range $2.1\times10^5 < Re\,\omega' < 1\times10^6$ can be correlated by

$$Nu = Pr^{0.3}\left[23.0 + \frac{5.6[Re\,\omega'\times10^{-5}-2]}{1+0.17(Re\,\omega'\times10^{-5}-2)}\right]. \tag{12}$$

The majority of the conditions considered here in the present study exceed the valid range of this correlation. At the lowest input rate however, $Re\,\omega' = 7.9\times10^5$ and Eq. (12) predicts $Nu = 38.3$ in the single-phase region. Referring to Table 4, (which presents data at a much higher input rate) we find that Eq. (12) over-predicts the heat transfer for $\gamma < 0.5$ by a factor of 2.

In the single-phase region, $\gamma < 0.5$, the second column of Table 4 indicates that the pulsating flow enhances heat transfer from 1.5 to 1.8 times over that for steady flow at an equivalent mass flow rate. Column three indicates that the Arpaci correlation for pulsating, single-phase flow over-predicts the heat transfer in this single-phase region of the tailpipe (ratios < 1).

Table 4
Experimentally determined averaged Nusselt number enhancement (values have been averaged over all eight input rates)

$\gamma = z/L$	Nu_i/Nu_{DB} steady single-phase	Nu_i/Nu_{AR} pulsating single-phase	Nu_i/Nu_{CH} steady two-phase
0.1[a]	4.4	2.1	
0.2	1.8	0.8	
0.3	1.5	0.7	
0.4	1.8	1.0	
0.5	2.1	1.2	0.4
0.6	2.0	1.3	0.4
0.7	3.0	2.0	0.7
0.75	3.7	2.6	0.8
0.8	5.0	3.7	1.1
0.833	6.2	4.7	1.4
0.866	9.0	6.2	1.9
0.9	10.3	8.3	2.5
0.933	12.4	10.2	3.0
0.966	11.1	9.6	2.7
0.99	9.0	8.0	2.3

[a] Enhancement ratios at this measurement location are suspect due to nonuniformities in external flow.

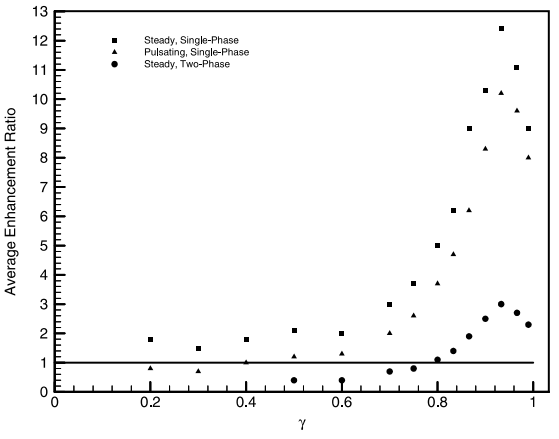

Fig. 11. Average heat transfer enhancement for two-phase pulsating flow over steady, pulsating, and condensing flows.

In the two-phase region of the tailpipe, $0.5 < \gamma < 1$, a number of conclusions can be drawn. First, in the transitional region (near $\gamma = 0.5$) the Arpaci correlation under-predicts the heat transfer enhancement while the Chato correlation for steady condensing flow over-predicts the heat transfer enhancement. This is easily explained by recognizing that the Chato correlation was developed for film condensation. In this transitional region of the pipe, condensation has only begun to occur so it is unlikely that the interior of the pipe is fully wetted (as suggested by flow visualization results). Third, towards the exit of the pipe (near $\gamma = 0.9$), both the Arpaci and Chato correlations under-predict the heat transfer which is enhanced over 10 times compared to steady, single-phase heat transfer. Referring to the last column of the table we see that past $\gamma = 0.8$, the Chato correlation for film condensation under-predicts the heat transfer. As discussed in conjunction with Fig. 7, the internal two-phase flow regime changes near this location. It is theorized that the condensate film begins to break up due to a combination of thickness and end effects. This breakup, entrainment, and the associated increased radial mass transport leads to the large heat transfer enhancement near the exit of the tailpipe.

5. Conclusions

Experimental measurements of internal heat transfer coefficients for fully reversing single-phase and two-phase circular pipe flow in the tail pipe of a pulse combustion furnace are presented. Comparisons made with existing heat transfer correlations for steady, pulsating, and filmwise condensing flows showed little agreement with the experimental data, as expected. Flow pulsation was shown to enhance heat transfer over steady-state predictions for all experimental conditions considered. Enhancement ratios greater than 12 times steady-flow predictions were observed in regions of pulsating, condensing flow. Heat transfer correlations are either nonexistent or unable to predict the experimental results obtained in this study. Further work, which spans a greater range of pulsation amplitude, pulsation frequency, and Reynolds number is needed to develop a heat transfer correlation with improved predictive power in pulsating, single- and two-phase flows.

References

[1] R.C. Martinelli, M.K. Boelter, S. Yakahi, Heat transfer to a fluid flowing periodically at low frequencies in a vertical tube, Trans. ASME 65 (1943) 789–798.

[2] J.E. Dec, J.O. Keller, V.S. Arpaci, Heat transfer enhancement in the oscillating turbulent flow of a pulse combustor tail pipe, Int. J. Heat Mass Transfer 35 (1992) 2311–2325.
[3] D.O. Barnett, R.I. Vachon, An analysis of convective heat transfer for pulsating flow in a tube, in: Proceedings of the Fourth International Heat Transfer Conference, Paris, 1970.
[4] I. Celik, Y.Z. Wang, Heat release and frictional effects on wave propagation in the tail pipe of pulsed combustors, in: Proceedings of the 1988 Pressure Vessels and Piping Conference, Pittsburgh, PA, 1988, pp. 1–6.
[5] A.A. Al-Haddad, N. Al-Binally, Prediction of heat transfer coefficient in pulsating flow, Int. J. Heat Fluid Flow 10 (1989) 131–133.
[6] G.K. Hargrave, J.K. Kilham, A. Williams, Operating characteristics and convective heat transfer of a natural-gas-fired pulsating combustor, J. Inst. Energy 59 (1986) 63–69.
[7] A.A. Al-Haddad, G.A. Coulman, Experimental and theoretical study of heat transfer in pulse-combustion heaters, in: Proceedings of Symposium on Pulse Combustion Applications, 1982, pp. 5-1 to 5-15.
[8] V.I. Hanby, Convective heat transfer in a gas-fired pulasting combustor, J. Eng. Power 91 (1969) 48–52.
[9] R.S. Gemmen, J.O. Keller, V.S. Arpaci, Pulse combustion: numerical analysis of droplet mass transfer enhancement, in: Proceedings of the 1990 Winter Annual Meeting of the ASME, vol. 16, ASME, New York, 1991, pp. 81–90.
[10] R.S. Gemmen, J.O. Keller, V.S. Arpaci, Heat/mass transfer from a cylinder in the strongly oscillating flow of a pulse combustor tailpipe, Combust. Sci. Technol. 94 (1993) 103–130.
[11] J.E. Dec, J.O. Keller, Pulse combustor tail-pipe heat-transfer dependence on frequency, amplitude, and mean flow rate, Combust. Flame 77 (1989) 359–374.
[12] V.S. Arpaci, J.E. Dec, J.O. Keller, Heat transfer in pulse combustor tailpipes, Combust. Sci. Technol. 94 (1991) 131–146.
[13] K. Temple, Thermal and acoustic model of a Helmholtz type pulse combustion furnace, Ph.D. Thesis, Purdue University, West Lafayette, IN, 1996.
[14] S.E. Hommema, Condensation heat transfer in pulsating flow, Master's Thesis, Department of Mechanical Engineering, Purdue University, West Lafayette, IN, 1997.
[15] W.W. Akers, H.F. Rosson, Condensation inside a horizontal tube, Chem. Eng. Prog. Symp. Ser. 30 (1960) 56.
[16] J.C. Chato, Laminar condensation inside horizontal and inclined tubes, J. ASHRAE 4 (1962) 52.
[17] S. Bae, J.S. Maulbetsch, W.M. Rosenhow, Refrigerant forced-convection condensation inside tubes, Technical Report 79760-59, Heat Transfer Laboratory, Massachusettes Institute of Technology, 1969.
[18] D.P. Traviss, W.M. Rohsenow, A.B. Baron, Forced convection condensation inside tubes, a heat transfer equation for condenser design, ASHRAE Trans. 79 (1973) 157–165.
[19] H. Jaster, P.G. Kosky, Condensation in a mixed flow regime, Int. J. Heat Mass Transfer 19 (1976) 95–99.
[20] T.H. Lyu, I. Mudawar, Determination of wave-induced fluctuations of wall temperature and convection heat transfer coefficient in the heating of a turbulent falling liquid film, Int. J. Heat Mass Transfer 34 (1991) 2521–2534.
[21] J.M. Mandhane, G.A. Gregory, K. Aziz, A flow pattern-map for gas–liquid flow in horizontal pipes, Int. J. Multiphase Flows 1 (1974) 537–553.
[22] A. Zhukauskas, Heat transfer from cylinders in cross-flow, in: J.P. Hartnett, T.F. Irvine Jr. (Eds.), Advances in Heat Transfer, vol. 8. Academic Press, New York, 1972.
[23] J.S. Truelove, A mixed gray gas model for flame radiation, Technical Report AERE-R-8494, United Kingdom Atomic Energy Authority Report, Harwell, 1976.
[24] F.P. Incropera, D.P. Dewitt, Fundamentals of Heat and Mass Transfer, Wiley, New York, 1990.